

Assessing synoptic wind hazard in Australia utilising climate-simulated wind speeds

L.A. Sanabria* and Cchet, R.P.

Risk and Impact Analysis Group, Geoscience Australia, Canberra, Australia

(Received March 4, 2011, Revised June 24, 2011, Accepted July 20, 2011)

Abstract. Severe wind is one of the major natural hazards in Australia. The component contributors to economic loss in Australia with regards to severe wind are tropical cyclones, thunderstorms and sub-tropical (synoptic) storms. Geoscience Australia's Risk and Impact Analysis Group (RIAG) is developing mathematical models to study a number of natural hazards including wind hazard. This paper discusses wind hazard under current and future climate conditions using RIAG's synoptic wind hazard model. This model can be used in non-cyclonic regions of Australia (Region A in the Australian-New Zealand Wind Loading Standard; AS/NZS 1170.2:2011) where the wind hazard is dominated by synoptic and thunderstorm gust winds.

Keywords: Australia; natural hazard; climate simulation; synoptic wind; wind hazard.

1. Introduction

The need to develop a new approach to understand and manage the risk posed by natural hazards in Australia has been acknowledged by Australian Federal and State governments. To this effect the Council of Australian Governments (COAG) commissioned a review of natural disaster relief arrangements in June 2001. A report with the results of the review was published by the Department of Transport and Regional Services in early 2004 (DOTARS 2004). The report proposes a fundamental shift in focus beyond relief and recovery towards cost-effective, evidence-based disaster mitigation. Consequently, while disaster response and reaction plans remain important, research has been directed towards anticipation and mitigation of natural hazards.

In this context Geoscience Australia (GA) is developing risk models and innovative approaches to assess the potential losses to Australian communities from a range of sudden impact natural hazards (Middelmann 2007). Severe wind is one of the major hazards facing Australia. While cyclonic winds are the major source of wind hazard in the northern states, non-cyclonic winds driven by synoptic lows, thunderstorms and tornadoes affect the southern states. Chen (2004) calculated that thunderstorms contributed about 8% of building damages in Australia during the 20th century; tornadoes contributed 4% and tropical cyclones 30%.

This paper presents the methodology developed to assess synoptic wind hazard in the non-cyclonic regions of Australia. The model was initially developed for observational data (i.e.,

* Corresponding author, Dr., E-mail: augusto.sanabria@ga.gov.au

anemometer records provided by the Bureau of Meteorology (BoM) and later extended to gridded data produced by a high resolution climate model. The high resolution climate model used in this project is CSIRO's Conformal Cubic Atmospheric Model (CCAM) (McGregor 2001). The latter approach allows the analyst to study wind hazard over a region. It can also be used to assess the impact of climate change on wind hazard.

To illustrate the methodology, hazard estimation for current and future climate conditions for the Australian state of Tasmania is presented. Currently only with gusts associated with synoptic winds are considered as CCAM provides hourly mean wind speed at a resolution of 14 km (average of six minute time steps) which do not explicitly resolve thunderstorms.

2. Model description

The synoptic wind hazard model comprises three components developed at GA in recent years:

- a statistical model to calculate wind hazard;
- a technique to extract wind speed and direction from CCAM; and
- a Monte Carlo (MC) model to calculate gust wind speed from mean wind speed.

Observed gust and mean wind speeds were extracted from the half-hourly wind dataset provided by BoM from anemometer records. The mean wind speeds in the dataset are the average wind speeds over the last 10 minutes prior to recording time. The gust wind speed is the maximum wind gust (three second average) of the last 10 minutes prior to recording time (BoM 2006).

2.1 Statistical model

The core of this model is the calculation of return periods (RP) for gust wind speed by fitting Extreme Value Distributions (EVD) to a given wind speed dataset. There are two basic methods to fit an EVD to a given dataset:

- a) The 'block maxima' method in which a number of EVDs are fitted to the annual maxima (the EVD used in this case are the generalised extreme value distributions).
- b) The 'Peaks over threshold' method in which the Generalised Pareto Distribution (GPD) is fitted to values exceeding a given threshold (Coles 2001).

The latter is the preferred method when maximum daily observations are available (Holmes and Moriarty 1999).

The major limitation of the GPD in practical work is the selection of the appropriate threshold 'u' for the given dataset. Only values above the threshold are considered for fitting the GPD. For this reason, the GPD is very sensitive to the threshold selection. To illustrate the problem, consider the curves of wind speed return period using the Sydney airport maximum daily wind speed dataset for 1939-2005 as shown in Fig. 1. The curves were generated by fitting GPD distributions with different thresholds 'u'. Table 1 shows the threshold used, the number of observations in the dataset exceeding the threshold and the shape parameter of the GPD for that threshold.

Selecting the appropriate threshold can be a very difficult task. Although there are methods to help modellers with the selection process they are mostly visual, subjective techniques, prone to producing inaccurate results and inappropriate for large scale applications. Hence to accurately model wind speeds using GPD distributions it is necessary to develop a technique for automatic

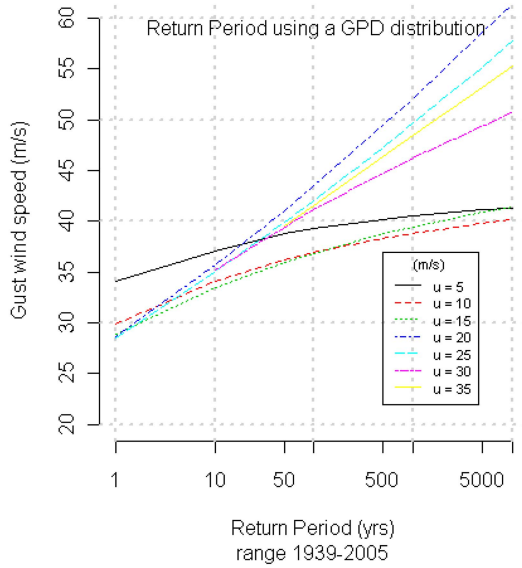


Fig. 1 GPD threshold sensitivity (using Sydney airport data)

Table 1. GPD sensitivity

| u (m/s) | Number of observations $> u$ | Shape parameter |
|-----------|------------------------------|-----------------|
| 5 | 23584 | -0.216 |
| 10 | 15788 | -0.168 |
| 15 | 5988 | -0.125 |
| 20 | 1574 | 0.043 |
| 25 | 252 | 0.033 |
| 30 | 38 | -0.067 |
| 35 | 6 | 5.253 |

selection of the appropriate threshold for a given dataset. One such technique developed for application to large gridded datasets is briefly described below.

2.1.1 Algorithm for automatic selection of threshold

The algorithm was developed by observing that there are two different sub-sets in Fig. 1: Sub-set 1 (with $u = 20, 25, 35$ m/s) is characterised by a shape parameter greater or equal to 0 which produces unbounded curves; these types of curves are inappropriate for modelling wind speed which is a naturally bounded phenomenon (Lechner *et al.* 1992). Sub-set 2 ($u = 5, 10, 15, 30$) m/s is characterised by a negative shape parameter which results in bounded curves appropriate for modelling wind speed; for this reason we call this the sub-set of *feasible* curves. Notice however that the curves produced by thresholds 5, 10 and 15, are flat with quick convergence to a very low speed value and hence are not appropriate for modelling wind hazard which depends on the high wind speed values. From Fig. 1 it is clear that the most appropriate threshold from those shown in Fig. 1 is $u = 30$ (m/s) which produces a bounded curve (one which asymptotically converges to a

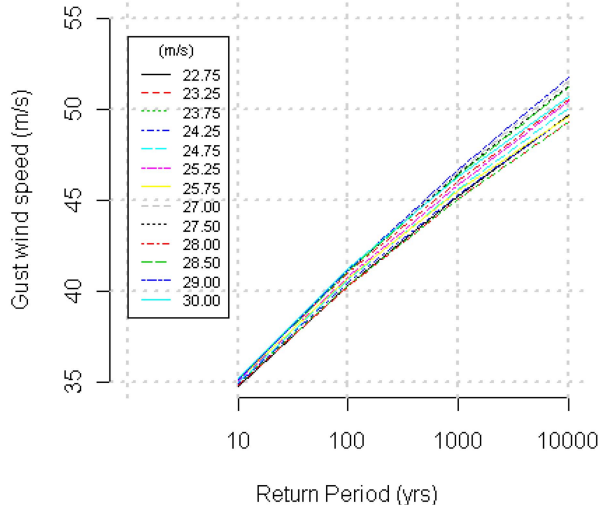


Fig. 2 Automatic threshold selection algorithm

limiting value) with the highest bounded return period of wind speed.

The algorithm generates a sub-set of *feasible* RP curves in steps of 0.25 (m/s) and selects the appropriate threshold for modelling the given dataset within this sub-set. It is generally the threshold producing the highest return period curve (i.e., the most conservative curve), which is employed for hazard determination. Based on return periods of observed wind speeds generated for a number of BoM datasets, a set of rules for selection of the appropriate threshold were compiled and coded to produce the automatic algorithm. Fig. 2 shows the selection algorithm at work using the same dataset as above; Feasible RP curves for threshold increases in steps of 0.25 (m/s) have been generated (the corresponding thresholds in m/s are shown in the left hand side table). In this case the algorithm returns 29.0 (m/s) as the appropriate threshold to fit the GPD to the given dataset as it produces the bounded RP curve with the highest asymptote. This RP curve compares well with the RP calculated from observed data (Sanabria and Cechet 2007).

For wind hazard applications it is important to separate the wind dataset into its component mechanisms (i.e., tropical cyclones, thunderstorms, tornadoes and synoptic winds). The importance of this approach concerns not only the physical characteristics of the component mechanisms but also the specific hazard that they pose to people and the built environment. The Statistical Model can separate these components using the weather description dataset also provided by BoM. Fig. 3 illustrates the case: the Sydney Airport wind speed dataset has been separated into thunderstorm and synoptic winds and RP curves using the GPD distribution have been calculated for each component. The RP curve based on the original complete dataset, called ‘combined winds’, is also shown.

2.2 Technique to extract wind speed and direction from CCAM

The availability of a fast and automatic algorithm for calculation of RP curves using a GPD allows us to obtain RP curves for a given region rather than at a single recording station. For climate simulation models a region is represented as a polygon consisting of a number of cells; the higher the grid resolution the higher the number of cells. To illustrate the application of the

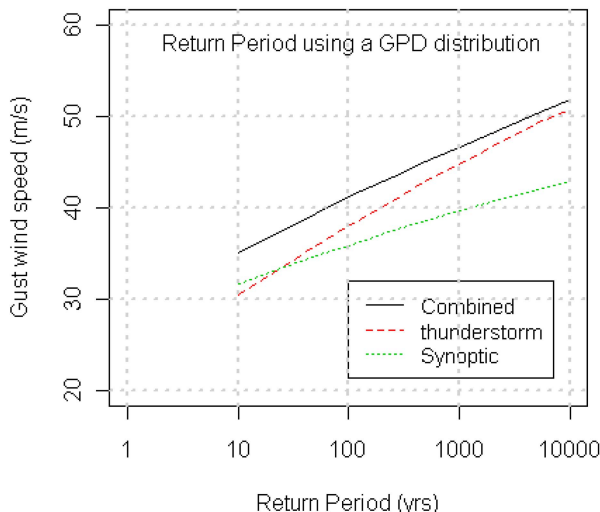


Fig. 3 Separation of wind components (Sydney airport)

statistical model to a grid, consider the state of Tasmania, south of the Australian mainland. Mean wind speeds produced by CCAM were extracted and used to calculate wind hazard over this area.

Simulations focusing on Tasmania, for the period 1961 to 2100, were generated by the Climate Futures for Tasmania project (CFT) to a grid with resolution of 0.1×0.1 degrees. Six coupled general circulation models (CGCM; see Table 2) were used to drive these simulations (Corney *et al.* 2010). In addition, each CGCM was forced by two IPCC (Intergovernmental Panel of Climate Change) greenhouse gas emission scenarios (B1 and A2) (IPCC 2000). Fig. 4 shows the elevation contour map of the Tasmanian region.

10-meter height hourly mean wind speeds from each of the six climate simulations were extracted using the NCO tools (NCO 2012). Then the hourly mean wind speeds extracted in each cell were transformed to maximum daily mean wind speeds using the R package ‘zoo’ (Zeileis and Grothendieck 2005). Extreme value distributions were then used to derive return period of wind speeds in each cell based on the modelled data. Fig. 5 shows the six model average exceedance level of mean wind speed corresponding to the 500-year RP for Tasmania. This RP was selected to illustrate the methodology because this is the design RP wind speed for residential structures used in Australia.

For model validation, three BoM recording stations were selected: Hobart, Launceston and

Table 2. Parent model (driver) for CCAM simulations

| CCAM “parent model” (driver) | Institution | Abbreviation |
|------------------------------|--|--------------|
| CSIRO mark 3.5 | CSIRO (Australia) | Mk3.5 |
| ECHAM 5 | Max-Planck Institut (Germany) | ECHAM5 |
| GFDL_CM 2.0 | Princeton Univ. /NOAA (USA) | GFDL2.0 |
| GFDL_CM 2.1 | Princeton Univ./NOAA (USA) | GFDL2.1 |
| MIROC 3.2 MEDRES | Centre for Climate System Research (Japan) | MIROC3 |
| UK Hadley_CM3 | Hadley Centre Met Office (UK) | UKhad |

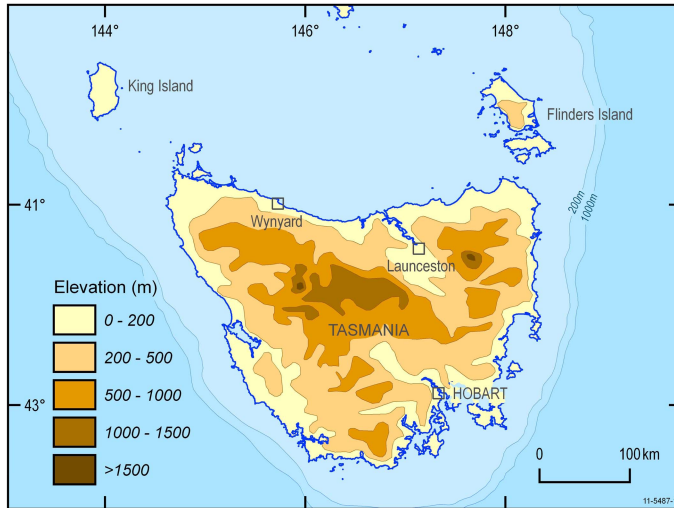


Fig. 4 Elevation contour map of Tasmanian region

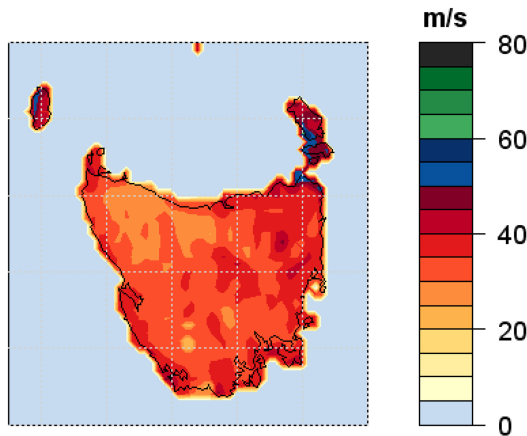


Fig. 5 Six model average 500-yr RP of mean wind speed, current climate

Wynyard Airports (shown by the squares in Fig. 4). These sites were selected because their weather observing stations and anemometer measurements are located at airports, avoiding the problem of the urban environment or trees affecting the instruments, and also due to these sites having long gust wind speed records.

2.3 Monte Carlo method to generate gust wind speeds

The wind map presented in Fig. 5 shows only RP of mean wind speed. Severe wind hazard requires however RP of gust wind speeds. A Monte Carlo-based technique (MC) to generate wind gust from mean wind speeds has been developed (Sanabria and Cechet 2010).

The MC works by simulating the physics of wind generation for synoptic wind conditions. It assumes that surface wind gusts result from the deflection of air parcels flowing higher in the boundary layer, which are brought down by turbulent eddies (Brasseur 2001). The method

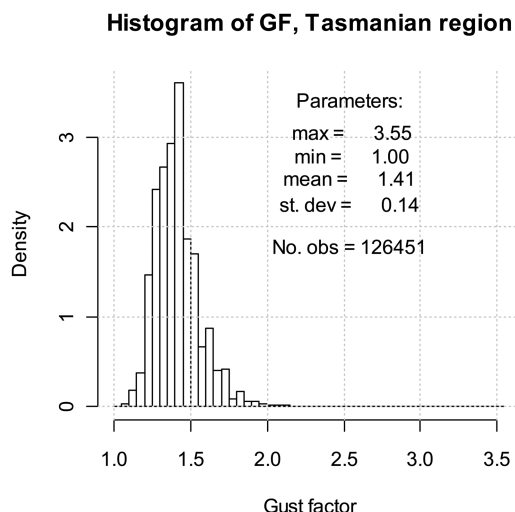


Fig. 6 Tasmanian regional gust factor (calculated from the BoM datasets)

separately takes into account the mean wind and the turbulent structure of the atmosphere. Turbulence is represented by the gust factor. The process consists of the probabilistic combination of the mean wind speed and the empirical gust factor distribution functions to produce the gust wind speed distribution.

2.3.1 Gust factors (GF)

The gust factor (GF) is defined as the ratio of maximum wind speed (gust) and mean wind speed for the same time period (generally between one and ten minutes duration). For this study the GF was calculated from the half-hourly wind speed dataset described in Section 2.

In order to capture the regional characteristics of Tasmania, half-hourly observed datasets for the three selected stations were acquired from BoM. The datasets were joined to calculate a *regional* GF which was applied to all cells of the Tasmanian grid. This GF was used for the sampling process in the Monte Carlo simulation. Fig. 6 shows the histogram of the Tasmanian regional GF.

3. Results

3.1 Current Climate

The methodology was applied to the available Tasmanian climate simulations to obtain RP curves of gust wind speeds. Data from a 30-year window (1961-1990) was extracted from each of the six simulations for scenarios A2 and B1. Fig. 5 shows the six model average exceedance level of mean wind speed corresponding to the 500-year RP. Representative gust wind speeds in each cell were then generated from these mean wind speeds using the MC process discussed above and the corresponding RP curve calculated.

To correct the bias which exists when comparing area-averaged climate simulated and location-based wind speeds, the RP of gust wind speeds at the three selected stations were generated and a

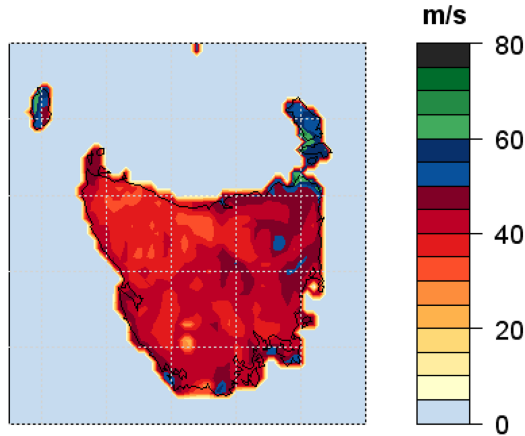


Fig. 7 Six model average 500-yr RP of gust wind speed, current climate

bias correction factor (ratio of observed RP and CCAM-generated RP) was calculated to force the CCAM-generated RP of gust winds at the selected stations to be similar to the observed ones; this correction factor was applied to all cells in the grid.

Fig. 7 shows the map of 500-year RP for (synoptic) gust speed under current climate conditions generated from Fig. 5 via the MC process. As expected the gust wind speeds follow closely the texture of the mean values (Fig. 5), in particular note the increase of synoptic wind speeds due to the effect of the mountain slope in both the south and north-east parts of Tasmania. This is consistent with detailed studies of the effect of mountain slopes on wind speeds (Holmes 2007).

All gust wind speed discussed here are over open terrain, i.e., they do not include regional characteristics such as terrain type, topography or wind direction. In practical applications these characteristics are taken into account by calculating wind multipliers to adjust the raw wind speeds to site specific conditions (Cechet *et al.* 2010).

3.2 Future Climate

To gain some insight into possible future extremes with regards to gust wind speeds, climate simulated daily maximum mean wind speeds from eight 20-year time-slices (windows) from 2010 to 2100 were extracted in each cell of the grid. This was undertaken for both the IPCC scenarios B1 and A2 utilising the six CCAM climate simulations. Their corresponding gust wind speeds were calculated using the MC procedure described above and RP curves for these 20-year windows (employing the statistical model) were generated. Large differences between each of the six simulations were noticed as discussed in the next section. The six model average RP was used in this project in order to reduce this (epistemic) uncertainty. Figs. 8 and 9 show the six model average gust wind speed exceedance level corresponding to the 500-year RP for the [2031-2050] and [2081-2100] windows. The RPs have been corrected using the bias correction factor discussed in Section 3.1.

Figs. 8 and 9 show that in general the wind hazard increases in the Tasmanian region for the time slices considered. However the increase is not uniform across the state; it is more marked in the north-east and north-west where orography is greatest, see Fig. 4. From Fig. 9 it is possible to see a progressive increase with time (i.e., the wind hazard increase is more pronounced by the end of the 21st century). Note that the white colour in Flinders Island, north of Tasmania, represents gust wind

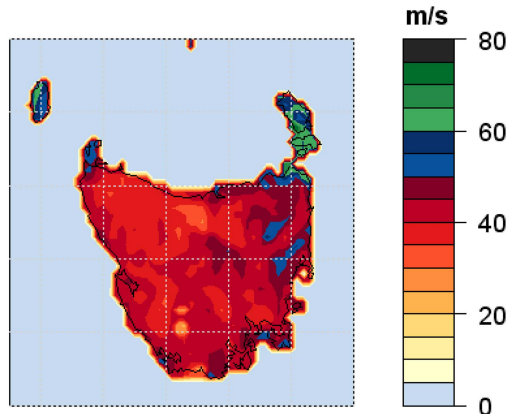


Fig. 8 Six model average 500-yr RP of gust wind speed, A2, 2031-2050

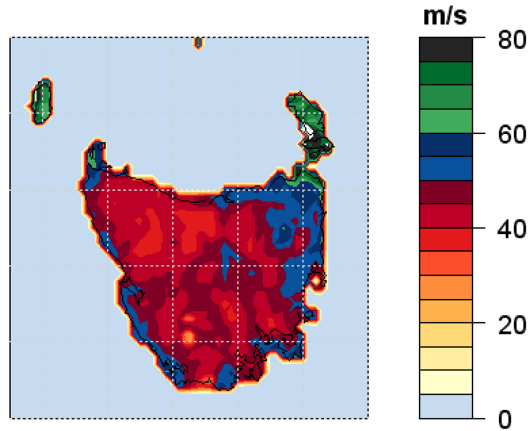


Fig. 9 Six model average 500-yr RP of gust wind speed, A2, 2081-2100

speeds greater than 80 m/s, associated with a single 1000 metre mountain adjacent to the sea.

An improved appreciation of the change in wind hazard can be obtained by showing a map of the percentage difference of future wind hazard compared to hazard under current climate. The corresponding map showing the difference between [2081-2100] and current climate is presented in Fig. 10(b). The former shows small increases in the regions of high wind hazard, in the north-east and north-west of the state; and a reduction of wind hazard in the south-east. Fig. 10(b) confirms that the hazard increases progressively with time; and that there is a small increase in wind hazard by the end of the century particularly in the north-east and north-west of the state.

It is also interesting to observe the difference in wind hazard when B1 scenario (a low greenhouse gas emissions scenario) is compared with the A2 scenario (Fig. 10(c)). This figure shows many spatial similarities when compared with Fig. 10(b). The increase in hazard when using a higher emissions scenario (A2) results in an increase in wind hazard in the regions of high hazard (north-east and north-west) and also in the south-west. This difference in the increase between the two scenarios is much lower than the increase of hazard presented in Fig. 10(b) (A2 scenario; 2080-2100), i.e., the hazard increase by the end of the century appears to be a function of the CO₂ emissions in the atmosphere.

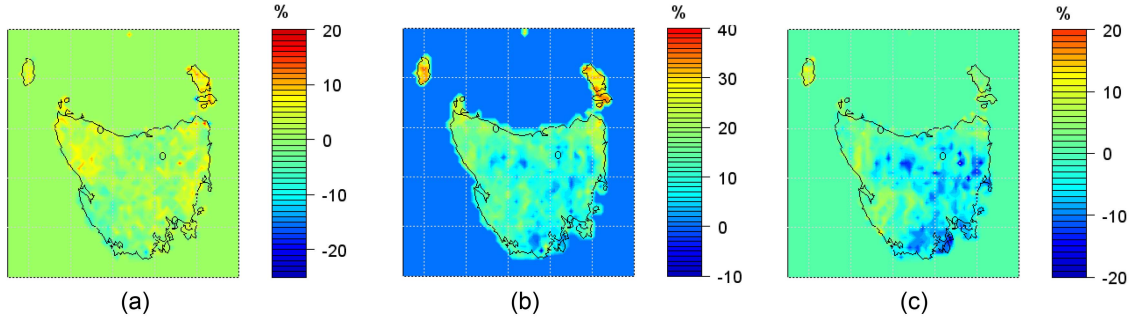


Fig. 10 (a) Difference in % between the 500-yr RP of gust speeds at 2031-2050 and current climate, (b) difference in % between the 500-yr RP of gust speeds at 2081-2100 and current climate and (c) difference in % between B1 and A2 scenarios for the 500-yr RP of gust speeds at 2081-2100

3.3 Long-term trend in wind hazard

The long-term trend of gust wind hazard in Tasmania is considered by examining the 500-year RP of gust wind speeds for the time slices explained above (scenario A2) corresponding to the locations of the Hobart and Launceston weather observing stations, located in the state's main cities (see Figs. 11 and 12). The RP values from each simulation have been standardised for the current climate by using the expression,

$$\text{RP_standard} = (\text{RP_mod}_j \text{time_slice}_k) / \text{RP_mod}_j \text{curr}$$

where: $\text{RP_mod}_j \text{curr}$ = Gust wind speed RP of current climate from model "j"

$\text{RP_mod}_j \text{time_slice}_k$ = Gust wind speed RP of model "j" at time slice "k"

Figs. 11 and 12 present the standardized 500-year RP values ("stand. RP"), where the mid point

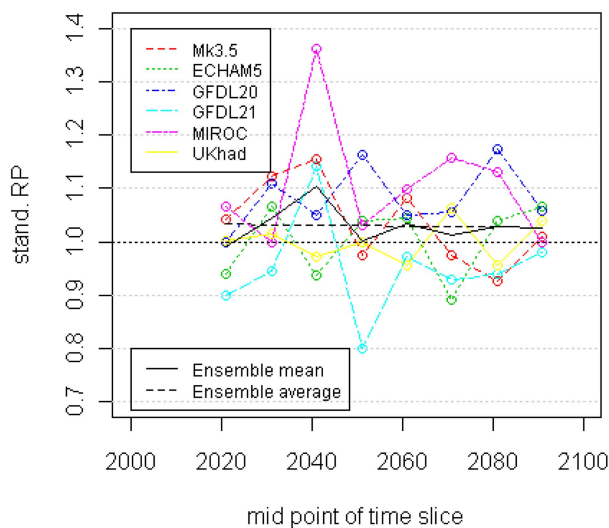


Fig. 11 Long-term trend of the 500-yr RP of gust wind speeds at Hobart station

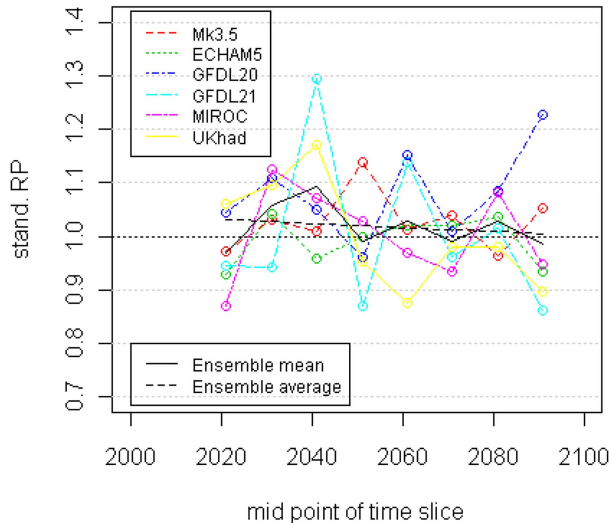


Fig. 12 Long-term trend of the 500-yr RP of gust wind speeds at Launceston station

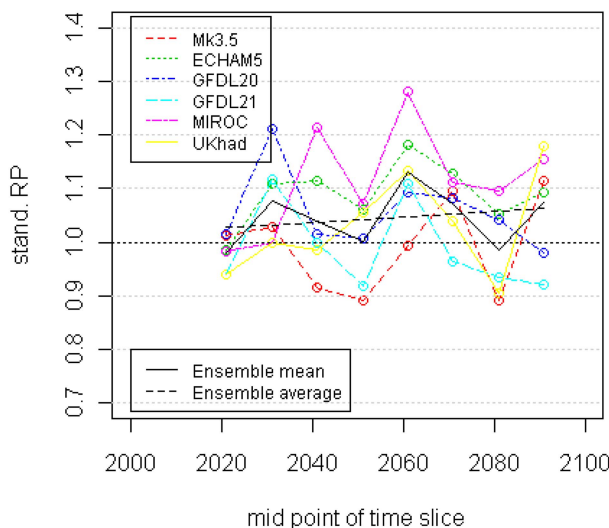


Fig. 13 Long-term trend of the 500-yr RP of gust wind speeds at Cranbrook

of the time slice is shown in these figures and the first point corresponds to current climate. To facilitate reading of the plot, a line has been drawn through the RPs and different line types have been used for each model. We observe that most model results are located above the "1.0" line, i.e. the models predict an increase of wind hazard with respect to current climate. There are however large differences in the level of increase. GFDL20, for instance, projects a substantial increase of wind hazard in Launceston by the end of the century (more than 30%) whilst GFDL21 projects a reduction of around 10% (Fig. 12).

The black lines show the ensemble mean and ensemble average. The former is the mean value of the RPs calculated from the six models and is shown with the full line, the latter is shown using a

Table 3 LR parameters for ‘ensemble average’ (scenario A2) for the Hobart, Launceston and Cranbrook regions in Tasmania.

| Location | Slope estimate | 95% CI lower | 95% CI upper |
|------------|----------------|--------------|--------------|
| Hobart | 0.0013 | -0.0105 | 0.013 |
| Launceston | -0.0014 | -0.0150 | 0.012 |
| Cranbrook | 0.0065 | -0.0107 | 0.024 |

dashed line and it is the linear regression (LR) calculated from all RP values in the plot. The analysis was repeated for the town of Cranbrook in the east of the state, a region of high hazard. The long-term trend in this region of Tasmania is for an increase in wind hazard as shown in Fig. 13 (A2 scenario). The Cranbrook region’s ensemble average indicates a larger wind hazard increase than in the other locations; about 7% by the end of the century.

Table 3 shows the slope parameter (trend over 21st century) of the ensemble average (LR) for each of the three locations considered, with their 95% confidence interval (CI). The linear regression for Hobart and Cranbrook have a small positive slope indicating a small increase in the long-term hazard, whilst for Launceston a small negative slope indicates a small reduction in hazard. It should be noted that based on all model results for all three locations that there is a large CI for the future trend (slope), indicating a large uncertainty about the true long-term trend of synoptic wind hazard at these stations. None of the trends are significant at the 95% confidence level (i.e., either positive or negative).

3.4 Application to codification

In practice wind engineers want to know the RP of gust wind speeds at a given location. Here we present the RP of observed and CCAM-modelled wind hazard at the Launceston airport observing station. We calculated the six-model average RP of gust wind speeds for a wide range of years (50 to 2000). Fig. 14 shows the RP curves for observed and three time-slices: current climate [1961-1990], [2041-2060] and [2081-2100]. For comparison purposes the AS/NZ standard (AS/NZS 1170.2:2011) RP of wind speeds for region A is also presented. Fig. 14 shows that CCAM-modelled RP of gust speeds for current climate are higher than those observed especially at low RP. For wind hazard we are more interested in the high values of RP and they tend to be closer to the observed values. The progressive increase of wind hazard with time (model ensemble average) discussed in the last section is also present here; RP for [2041-2060] are higher than RP for current climate; whilst the RP for [2081-2100] are the highest RP shown in the plot. It is interesting to observe the location of the RP for the wind loading standard curve (AS/NZS 1170.2:2011) which considers both synoptic and thunderstorm hazard. Based on the model ensemble average analysis for synoptic wind hazard and assuming that the thunderstorm hazard remains static for the Launceston region, we would be concerned that AS/NZS 1170.2:2011 is unlikely to remain a conservative estimate of the wind hazard well into the 21st century. However, the influence of climate change and the uncertain nature of the 21st century trend for the ensemble average of the synoptic wind hazard (discussed in Section 3.3) indicate that a cautious approach to codification is merited and further research on the impact of climate change on wind hazard is required.

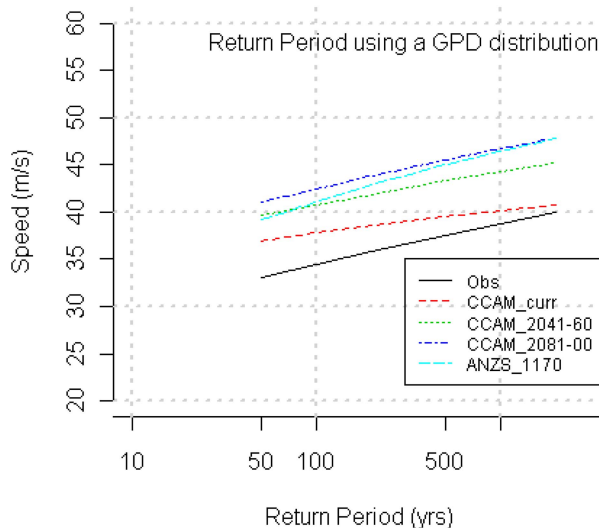


Fig. 14 RP of observed and modelled synoptic winds at Launceston station

4. Discussion

Climate change will result in global warming that will be expressed by significant regional and local differences in the magnitude of the warming. While the entire globe is expected to warm severe wind hazard is likely to show both regional increases and reductions. CSIRO climate change projections based on the IPCC Fourth Assessment Report (AR4) (IPCC 2007) indicate that Tasmania is one area within the Australian region that will experience an increased magnitude of severe winds (CSIRO 2007). This study showed seasonal changes in the 90th percentile mean 10 meter wind speed for the Tasmanian region. Increases in the wind extremes (peak gust) are also expected, and they may be greater than for the mean increase based on detailed modelling undertaken in other regional studies. The CSIRO study suggests a greater than 15% increase in wind speeds in the Winter, Spring and Summer seasons which should be of significant concern to emergency services and the community as a whole (impacts with regard to planning, building standards, agriculture, water resources are expected). The physical basis for this increase in wind hazard is that the synoptic “westerly stream weather” (i.e., cold fronts embedded in the mid-latitude westerly winds) will be influenced by an increase in the pressure gradient between the synoptic subtropical ridge, which climate models suggest is moving polewards (Hope *et al.* 2006, Hope 2006) and the polar front (i.e., maximum westerly winds) which are expected to remain approximately stationary (Gupta *et al.* 2009). Fig. 15 shows results from the IPCC AR4 models examining the change in the zonally averaged wind stress maximum position Tau (pos) versus the position of wind stress maximum (i.e., maximum westerlies) in the “current climate” control simulation. Little or no movement in the latitude of the maximum westerlies is shown indicating the likelihood of a tighter pressure gradient over the Tasmanian region (approx. 40-45 degrees South). Analysis of the CGCM model output used as input for the dynamic downscaling model output used for this project (Suppiah *et al.* 2007) indicates a general agreement regarding this broad climate trend. However, significant differences in model performance were evident (as is shown here for severe winds), hence we have provided ensemble averages to best inform trends in future severe wind hazard.

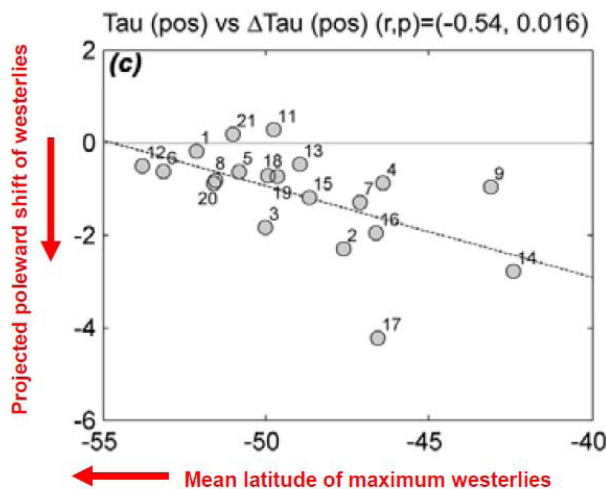


Fig. 15 Scatter plot from IPCC AR4 models of change in the zonally averaged wind stress maximum position Tau (pos) vs position of wind stress maximum (i.e., maximum westerlies) in the “current climate” control simulation. The latitude of the maximum westerlies is calculated from the zonally averaged depth-integrated zonal velocity (diagram reproduced from Gupta *et al.* 2009, Fig. 4(c)). The numbers next to the plotted circles refer to 1: Observed, and for the six models considered in this study; 6: Mk3.5, 7: GFDL2.0, 8: GFDL2.1, 16: MIROC3, and 18: ECHAM5 (UKhad not shown)

5. Conclusions

A computational methodology developed for assessing synoptic wind hazard in the non-cyclonic regions of Australia has been presented. The methodology, initially developed for observational data, has been applied to gridded data from climate models, which has enabled the regional study of synoptic wind hazard for both current climate and also for future climate scenarios extending to the end of the 21st century.

The methodology has been demonstrated by considering the current and future climate for the island state of Tasmania. Six climate models and two climate change scenarios (B1 & A2) have been considered. In general, the wind hazard increases in the Tasmanian region. However, the increase is not uniform across the state. The increase is most noticeable in the north-east and north-west where the orography is most significant. In general for the Tasmanian region, the ensemble average of all models considered (IPCC SRES A2 scenario) indicates a small increase in synoptic wind hazard for the 21st century in most regions. For the three locations within Tasmania considered here, there is a large CI for the 21st century trend (slope) when considering all models, indicating a large uncertainty about the true long-term trend of synoptic wind hazard at these stations. The trends for the three population areas considered are not significant at the 95% confidence level (i.e., either positive or negative); however this is not the case for the whole Tasmanian region.

References

AS/NZS 1170.2:2011 (2011), Australia/New Zealand Standards. Structural design actions. Part 2: Wind actions.

- Bureau of Meteorology (2006), Basic Climatological Station Metadata. Metadata compiled: Sept. 29, 2006.
- Brasseur, O. (2001), "Development & application of a physical approach to estimating wind gusts", *Mon. Weather Rev.*, **129**, 5-25.
- Cechet, R.P., Arthur, W.C., Wehner, M., Sanabria, L.A., Thomas, C., Nadimpalli, K., Power, L., Divi, C.B and Yang, T. (2010), "National wind risk assessment for the Australian region", *Proceedings of the 5th International Symposium on Computational Wind Engineering (CWE2010)*, Chapel Hill, North Carolina, USA, May.
- Chen, K. (2004), "Relative risks ratings for local government areas", *Risk Frontiers quarterly newsletter, Macquarie University, Australia*, **3**(3), March .
- CSIRO (2007), *Climate Change in Australia - Wind Speed*, Technical Report , Supplementary Material.
- Coles, S. (2001), *An Introduction to Statistical Modeling of Extreme Values*, Springer series in statistics, London, U.K.
- Corney, S., Katzfey, J., McGregor, J., Grose,M., Bennett, J., White, C.J., Holz, G. and Bindoff, N.L. (2010), *Climate futures for Tasmania technical report: methods and results on climate modelling*, Antarctic Climate and Ecosystems Cooperative Research Centre, Hobart, Tasmania.
- DOTARS (2004), *Natural Disasters in Australia – Review of mitigation, relief and recovery arrangements*, Report to the Council of Australian Governments (COAG).
- Gupta, A.S., Santoso, A.A., Taschetto, A.S., Ummenhofer, C.C., Trevena, J. and England, M.H. (2009), "Projected changes to the Southern Hemisphere ocean and sea ice in the IPCC AR4 climate models", *J. Climate*, **22**(11), 3047-3078.
- Holmes, J.D. and Moriarty, W.W. (1999), "Application of the generalised pareto distribution to extreme value analysis in wind engineering", *J. Wind Eng. Ind. Aerod.*, **83**(1-3), 1-10.
- Holmes, J.D. (2007), *Wind Loading of Structures*, 2nd Ed., Taylor & Francis.
- Hope, P.K. (2006), "Projected future changes in synoptic systems influencing southwest Western Australia", *Clim. Dynam.*, **26**(7-8), 765–780.
- Hope, P.K. Drosdowsky, W. and Nicholls, N. (2006), "Shifts in the synoptic systems influencing southwest Western Australia". *Clim. Dynam.*, **26**(7-8), 751–764.
- IPCC Special Report on Emission Scenarios SRES (2000), In: http://www.ipcc.ch/publications_and_data/publications_and_data_reports.shtml#2
- IPCC Fourth Assessment Report: (AR4): Climate Change (2007), In: http://www.ipcc.ch/publications_and_data/publications_and_data_reports.shtml
- Lechner, J.A., Leigh, S.D. and Simiu, E. (1992), "Recent approaches to extreme value estimation with application to wind speeds. Part I: the pickands method", *J. Wind Eng. Ind. Aerod.*, **41**(1-3), 509-519.
- McGregor, J.L. and Dix, M.R. (2001), *The CSIRO conformal-cubic atmospheric GCM. In IUTAM Symposium on Advances in Mathematical Modelling of Atmosphere and Ocean Dynamics*, (Ed., Hodnett, P.F.), Kluwer, Dordrecht, 197-202.
- Middelmann, M. (2007), Natural hazards in Australia. identifying risk and analysis requirements, Geoscience Australia, GeoCat # 6544.
- NetCDF Operator (NCO) Tools (2012), In: <http://nco.sourceforge.net/>
- Sanabria, L.A. and Cechet, R.P. (2007), "A statistical model of severe winds", Geoscience Australia, GeoCat # 65052.
- Sanabria, L.A. and Cechet, R.P. (2010), "Severe wind hazard assessment using Monte Carlo simulation", *Environ. Model. Assess.*, **15**(2), 147-154.
- Suppiah, R., Hennessy, K.J., Whetton, P.H., McInnes, K.L. Macadam, I. Bathols, J. Ricketts, J. and Page, C.M. (2007), "Australian climate change projections derived from simulations performed for the IPCC 4th assessment report", *Aust. Meteorol. Mag.*, **56**, 131-152.
- Zeileis, A. and Grothendieck, G (2005), "zoo: infrastructure for regular and irregular time series", *J. Stat. Soft.*, **14**(6), 1-27.